1   **Title: Manipulation of IRE1-dependent MAPK signaling by a Vibrio agonist-antagonist**

2   **effector pair**

3

4   **Authors:** Nicole J. De Nisco[1,2,3]†, Amanda K. Casey[1]†, Mohammed Kanchwala[4], Alexander E.

5   Lafrance[1], Fatma S. Coskun[5], Lisa N. Kinch[2], Nick V. Grishin[2,6], Chao Xing[4,7,8], Kim Orth[1,2,6]*

6   **Affiliations:**

7   [1]Department of Molecular Biology, University of Texas Southwestern Medical Center, Dallas,

8   TX, 75390

9   [2]Howard Hughes Medical Institute, University of Texas Southwestern Medical Center, Dallas,

10   TX, 75390

11   [3]Department of Biological Sciences, University of Texas at Dallas, Richardson, TX 75080, USA.

12   [4]McDermott Center for Human Growth and Development, UT Southwestern Medical Center,

13   Dallas, TX, 75390

14   [5]Department of Immunology, University of Texas Southwestern Medical Center, Dallas, TX,

15   75390

16   [6]Department of Biophysics and Biochemistry, University of Texas Southwestern Medical Center,

17   Dallas, TX, 75390

18   [7]Department of Bioinformatics, University of Texas Southwestern Medical Center, Dallas, TX,

19   75390

20   [8]Department of Population and Data Sciences, University of Texas Southwestern Medical

21   Center, Dallas, TX 75390

22   †Authors contributed equally to this work

23   *Correspondence may be addressed to Kim Orth (kim.orth@utsouthwestern.edu)

24 **Running Title**

25 Agonist-antagonist effectors manipulate host signaling
26

27 **Abstract:**

28 Diverse bacterial pathogens employ effector delivery systems to disrupt vital cellular processes

29 in the host (*1*). The type III secretion system 1 of the marine pathogen, *Vibrio*

30 *parahaemolyticus,* utilizes the sequential action of four effectors to induce a rapid, pro-

31 inflammatory cell death uniquely characterized by a pro-survival host transcriptional response (*2,*

32 *3*). Herein, we show that this pro-survival response is caused by the action of the channel-

33 forming effector VopQ that targets the host V-ATPase resulting in lysosomal deacidification and

34 inhibition of lysosome-autophagosome fusion. Recent structural studies have shown how VopQ

35 interacts with the V-ATPase and, while in the ER, a V-ATPase assembly intermediate can

36 interact with VopQ causing a disruption in membrane integrity. Additionally, we observe that

37 VopQ-mediated disruption of the V-ATPase activates the IRE1 branch of the unfolded protein

38 response (UPR) resulting in an IRE1-dependent activation of ERK1/2 MAPK signaling. We also

39 find that this early VopQ-dependent induction of ERK1/2 phosphorylation is terminated by the

40 VopS-mediated inhibitory AMPylation of Rho GTPase signaling. Since VopS dampens VopQ-

41 induced IRE1-dependent ERK1/2 activation, we propose that IRE1 activates ERK1/2

42 phosphorylation at or above the level of Rho GTPases. This study illustrates how temporally

43 induced effectors can work as in tandem as agonist/antagonist to manipulate host signaling and

44 reveal new connections between V-ATPase function, UPR and MAPK signaling.

45

46

47 **Importance:**

48 *Vibrio parahaemolyticus (V. para)* is a seafood-borne pathogen that encodes two Type 3

49 Secretion Systems (T3SS). The first system T3SS1 is thought to be maintained in all strains of *V.*

50 *para* to to maintain survival in the environment, whereas the second sytem T3SS2 is linked to

51 clinical isolates and disease in humans. Herein, we find that first system targets evolutionarily

52 conserved signaling systems to manipulate host cells, eventually causing a rapid, orchestrated

53 cells death within three hours. We have found that the T3SS1 injects virulence factors that

54 temporally manipulate host signaling. Within the first hour of infection, the effector VopQ acts

55 first by activating host surval signals while diminishing the host cell apoptotic machinery. Less

56 than an hour later, another effector VopS reverses activation and inhibition of these signaling

57 systems ultimately leading to death of the host cell. This work provides example of how

58 pathogens have evolved to manipulate the interplay between T3SS effectors to regulate host

59 signaling pathways.

60

61 **Introduction**

62 The seafood-borne pathogen, *Vibrio parahaemolyticus* (*V. para*), uses two needle-like type III

63 secretion systems (T3SS1 and T3SS2) to inject effectors into host cells to manipulate signaling

64 and cellular processes during infection (*2*). The *V. para* T3SS2 is found in clinical isolates, is

65 linked to disease in humans and has been shown to mediate invasion into mammalian host cells

66 (*4, 5*). By contrast, the T3SS1 is present in all *V. para* isolates and is thus believed to be essential

67 for survival in its environmental niche. This niche has been rapidly expanding due to the

68 warming of coastal waters contributing to the resurgence of *V. para* as a significant cause of

69 gastroenteritis world-wide (*6, 7*). Together, the *V. para* T3SS1 effectors orchestrate a temporally

3

70   regulated non-apoptotic cell death in cultured cells (*2*). The specific cell type that T3SS1 has

71   evolved to target in the environment remains undefined; however, its effectors target processes

72   that are conserved from yeast to humans (*2, 8-10*).

73   Cell death mediated by T3SS1 occurs in distinct and highly reproducible stages through the

74   temporal action of four known effectors: VopQ (VP1680), VPA0450, VopS (VP1686) and VopR

75   (VP1683) (Fig. 1A) (*2, 11*). Within 30 minutes of a synchronized infection, VopQ forms an

76   outward-rectifying channel in V-ATPase-containing membranes resulting in neutralization of the

77   compartment (e.g. vacuole or lysosome) and inhibition of membrane fusion (Fig. 1A) (*9, 12*).

78   These two activities inhibit autophagic flux, resulting in massive autophagosome accumulation

79   and contribute to a pro-inflammatory cell death within three hours(*13*). VPA0450 is a

80   phosphatidyl 5-phosphatase that hydrolyses $PI(4,5)P_2$ at about one hour after infection, resulting

81   in blebbing of the plasma membrane (Fig. 1A) (*14*). Soon after, VPA0450-mediated blebbing is

82   observed, VopS, a Fic (filamentation induced by cAMP) domain–containing protein, covalently

83   attaches an adenosine monophosphate (AMP) to a threonine residue in the switch 1 region of

84   Rho guanosine triphosphatases (GTPases) Rho, Rac and Cdc42. This modification, termed

85   AMPylation, inactivates the Rho GTPases thereby precipitating cytoskeletal collapse and cell

86   rounding, as well as inactivation of nuclear factor-kappaB (NF-κB) and mitogen activated

87   protein kinase (MAPK) signaling pathways (Fig. 1A) (*10, 15*). The fourth effector, VopR, causes

88   cell rounding around 90 minutes post infection, but its activity has remained elusive (*11*).

89   Despite the rapid, non-apoptotic cell death orchestrated by the T3SS1, our previous studies have

90   uncovered evidence that the T3SS1 rewires host gene expression to subvert cell death and

91   activate cell survival pathways, including MAPK signaling pathways**.** We performed a systems

92   level analysis of the temporal changes in host cell gene expression during *V. para* infection to

93   understand how the T3SS1 effectors work in concert to orchestrate cell death and subvert host

94   immune responses (*3*). The host transcriptional response to T3SS1 resulted in the activation of

95   host cell survival networks and repression of cell death networks (*3*).

96   Previously, it was found that VopQ was both necessary and sufficient for the accumulation of

97   LC3-positive autophagosomes as well as the deacidification of endolysosomal compartments.

98   These effects are caused by direct interaction between VopQ and the V_o subcomplex of the V-

99   ATPase. Recently, cryo-EM studies performed in our lab revealed extensive interactions

100   between VopQ and the c subunit of V_o V-ATPase that stabilize the insertion of VopQ in the

101   membrane alongside the V-ATPase (*16*). The interactions of VopQ with the c-ring of V_o is

102   predicted to form an unconventional membrane pore through the juxtaposition of charged resides

103   of VopQ against the hydrophobic lipid environment (*16*). This disruption is predicted to lead to

104   the deacidification of the lysosomal membrane. Remarkably, a fully functioning or assembled V-

105   ATPase at the vacuole is not necessary to induce VopQ toxicity in yeast. We found that VopQ

106   can interact with an assembly intermediate of the V-ATPase (V_o c-ring) in the ER resulting in

107   cell death (*16*). As VopQ forms a pore in target membranes, the ER membrane is compromised,

108   and this could lead to the induction of host cell signaling events including the unfolded protein

109   response (UPR).

110   Herein, we find that VopQ activates the IRE1 branch of the UPR in yeast and cultured cells. We

111   demonstrate that the activation of IRE1 by VopQ results in an activation of extracellular singal-

112   regulated protein kinase 1/2 (ERK1/2) signaling that is dependent on IRE1 kinase but not

113   nuclease activity. We also find that another T3SS1 effector VopS dampens VopQ-mediated

114   activation of ERK1/2 signaling by AMPylation-dependent inactivation of Rho GTPases, thereby

115   limiting the activation of ERK1/2 signaling to early infection time points. Taken together, our

116 work provides another example of the powerful interplay between T3SS effectors and how they

117 can temporally regulate host signaling pathways.

118

119 **Results**

120 *VopQ and VopS have antagonistic effect on T3SS1-specific pathway and network induction*

121 Previously, we discovered that the T3SS1 activates host cell survival networks and represses of

122 cell death networks. Since, autophagy is linked to pro-survival network signaling, our findings

123 led us to ask if VopQ could be responsible for pro-survival signals observed during infection. To

124 understand the contribution of individual effectors to the T3SS1-specific transcriptional

125 response, we characterized infection of primary human dermal fibroblasts (PHDFs) with *V. para*

126 strains carrying single-effector deletions for either *vopQ* or *vopS*. We chose this cell line so that

127 our data would be comparable with the data obtained in our previous transcriptomic analysis (*3*).

128 We included VopS because it targets Rho GTPases that regulate MAPK signaling (*15, 17*). We

129 used *V. para* strain, POR3, a derivative of the clinical strain RIMD2210633 that does not

130 produce functional hemolysins or a functional T3SS2 (*ΔtdhASΔvcrD2)*, but maintains an active

131 T3SS1 (*6*). This strain and its Δ*vopQ* and Δ*vopS* derivatives will be referred to herein as T3SS1$^+$,

132 T3SS1$^+$Δ*vopQ* and T3SS1$^+$Δ*vopS,* respectively (Table S1). As observed with previously

133 characterized cell types, cytotoxicity of PHDFs occurring within the first four hours of infection

134 was completely dependent on VopQ (Fig. S1A,B) (*2*). We then performed RNA-sequencing on

135 the PHDFs after 90 minutes of infection with *V. para* T3SS1$^+$, T3SS1$^+$Δ*vopQ* and T3SS1$^+$Δ*vopS*

136 strains. The sequencing data passed statistical quality control tests, and principal component

137 analysis indicated tight clustering of replicates (Fig. S2A). Complete differential expression data

138   is reported in Table S2, but for this study we focused on the 398 host genes previously found to

139   be differentially expressed specifically in response to the T3SS1 (*3*).

140   The hierarchically clustered expression heatmap in Fig. 1B illustrates how the T3SS1 causes

141   changes in expression of these 398 genes in the absence of either VopQ or VopS. Of these

142   T3SS1-specific genes, 146 were similarly differentially expressed in the uninfected (UN) vs.

143   T3SS1$^+$ and UN vs. T3SS1$^+\Delta vopQ$-infected cells, and 197 were similarly differentially expressed

144   in the UN vs. T3SS1$^+$ and UN vs. T3SS1$^+\Delta vopS$-infected cells (Fig. S2B, Table S3). 252 and 201

145   T3SS1-specific genes were either not differentially expressed or changed direction during

146   T3SS1$^+\Delta vopQ$ and T3SS1$^+\Delta vopS$ infection, respectively. Expression of many genes, especially

147   those within clusters 1 and 4, was oppositely affected during infection with T3SS1$^+\Delta vopQ$

148   compared to during infection with T3SS1$^+\Delta vopS$ (Fig. 1B, Table S3). Notably, expression of the

149   *EGR1* and *FOS* transcription factors, which are known to be regulated by MAPK signaling

150   pathways, was reduced in T3SS1$^+\Delta vopQ$-infected cells compared to T3SS1$^+$-infected cells, and

151   highly elevated by T3SS1$^+\Delta vopS$ infection (Table S3)(*18*). We validated these findings by

152   quantitative RT-PCR and using *V. para* strains deleted for multiple effectors (T3SS1$^+$

153    $\Delta vopQR\Delta vpa0450$ and T3SS1$^+$ $\Delta vopRS\Delta vpa0450$) and showed that VopQ is necessary and

154   sufficient for the elevated expression of both *FOS* and *EGR1* (Fig. S2C,D).

155   We next used Ingenuity Pathway Analysis (IPA) to understand how the activities of VopQ and

156   VopS contribute to the changes in host signaling events induced by the T3SS1 (Table S4). The

157   T3SS1-specific induction or repression of many pathways was dependent on VopQ and

158   enhanced in the absence of VopS (Fig. 1C). For example, induction of NF-kB signaling, actin

159   cytoskeleton signaling and Rho GTPase signaling by T3SS1 was greatly reduced in the absence

7

160   of VopQ and enhanced in the absence of VopS. These observations are consistent with the

161   opposing effects on differential expression patterns observed in Fig. 1B.

162

163   *VopQ induces pro-survival signaling networks*

164   To understand the relative contributions of VopQ and VopS to the host response to T3SS1 on the

165   network level, we used IPA to perform biological function network analysis. Previously, we had

166   shown that the T3SS1 activates cell survival networks and represses cell death networks(*3*).

167   Strikingly, this effect was completely lost during T3SS1$^+\Delta vopQ$ infection and amplified during

168   T3SS1$^+\Delta vopS$ infection (Fig. 1D, Table S5). Specifically, we observed a loss in cell survival and

169   viability signaling network activation and death and mortality signaling network repression in

170   PHDFs infected with *V. para* T3SS1$^+\Delta vopQ$ compared to *V. para* T3SS1$^+$ while infection with

171   T3SS1$^+\Delta vopS$ instead amplified these signaling changes (Fig. 1D). Interestingly, the apoptosis

172   signalling network, which is normally repressed during T3SS1$^+$ infection, was activated during

173   infection with T3SS1$^+\Delta vopQ$ (Fig. 1D). These data strongly a model in which the activity of

174   VopQ elicits significant transcriptional changes in the host cell that result in the activation of cell

175   survival and repression of cell death networks and that VopS functions to dampen this response.

176

177   *VopQ induces a pulse of ERK1/2 signaling that is dampened by VopS*

178   To further dissect VopQ's effect on host signaling pathways in mammalian cells, we continued

179   with a more genetically tractable model, mouse embryonic fibroblasts (MEFs). We characterized

180   the cytotoxicity of the *V. para* T3SS1$^+$ strain and its derivates in MEFs. The cell death induced

181   by the T3SS1 occurred over a similar timescale in MEFs as in PHDFs and was similarly

182   dependent on VopQ (Fig. S3A). This result was expected because the mechanism of T3SS1-

183   mediated cell death is conserved across diverse cell types (*2, 3, 9, 15*). We chose to examine the

184   ERK1/2 signaling pathway because the RNA-sequencing data suggested that VopQ activates

185   Rho GTPase signaling (Fig. 1C) and in previous work we demonstrated that T3SS1-induced

186   *EGR1* and *FOS* expression requires active MEK1/2, the kinase upstream of ERK1/2 (*3*).

187   Furthermore, as we did not observe agonist and antagonist effects of VopQ and VopS,

188   respectively, on the expression of c-Jun N-terminal kinase (JNK) signaling target genes, we

189   focused our analysis on the ERK1/2 pathway (Table S6).

190   To test if VopQ induces *EGR1* and *FOS* expression by activating the ERK1/2 MAPK pathway

191   early during infection, we starved MEFs to remove basal ERK1/2 phosphorylation, infected them

192   with *V. para* T3SS1^{+} or *V. para* T3SS1^{-} for 45, 60, 75 and 90 minutes, and probed for phospho-

193   ERK1/2 as well as for the presence of downstream Egr1 by Western blot. We found that the

194   T3SS1 induced a pulse of ERK1/2 phosphorylation that peaked around 45 minutes and had

195   completely disappeared by 90 minutes post infection (Fig. 2A). Total Egr1 protein levels began

196   to rise 60 minutes post infection and reached their maximum at 90 minutes post infection, which

197   is an expected pattern of expression when taking into account the time for transcription and

198   translation of the induced *Egr1* gene (Fig. 2B). Using the MEK1/2 inhibitor U0126, we found

199   that T3SS1-induced *Egr1* expression was similarly dependent on MEK1/2 activity in MEFs as

200   previously reported in PHDFs (Fig. S3B) (*3*).

201   We repeated the infection time course with the *V. para* T3SS1^{+}Δ*vopQ* strain and found that the

202   T3SS1-induced pulse of ERK1/2 phosphorylation was indeed dependent on VopQ as was the

203   increase in total Egr1 protein levels (Fig. 2C,D). When MEFs were infected with T3SS1^{+}Δ*vopS,*

204   we observed not only an amplified induction of ERK1/2 phosphorylation and Egr1 production,

205   but also an extended duration of ERK1/2 phosphorylation (Fig. 2C,D). This observation is

206 consistent with previous work that found that VopS's AMPylation of Rho GTPases inhibits host

207 ERK1/2 and c-Jun N-terminal kinase (JNK) MAPK pathways (*15*). This early pulse of VopQ-

208 dependent ERK1/2 MAPK signaling in MEFs is distinct from the previously reported VopQ-

209 dependent ERK1/2 phosphorylation in Caco-2 cells during late infection time points, 3-4 hours

210 post infection, as those assays were performed with *V. para* strains that encoded functional

211 T3SS1, T3SS2 and TdhAS hemolysins (*19*). Taken together, these data support the model that

212 the combined action of VopQ and VopS create a pulse of ERK1/2 MAPK signaling that is

213 restricted to early infection timepoints resulting in the controlled expression of downstream

214 transcription factors EGR1 and FOS.

215 If VopQ and VopS work together to fine-tune the host response, their co-occurrence in *Vibrio*

216 genomes containing the T3SS1 gene cluster would be predicted to be high. To test this, we used

217 the SyntTax server to identify all *Vibrio* strains that retained synteny in the T3SS1 gene

218 neighborhood (Table S7). We identified 58 *Vibrio* strains representing 8 species containing the

219 T3SS1 gene cluster and found that 91.4% of genomes containing *vopQ* also contained *vopS*

220 (53/58) (Table S7). We found that these genes co-occur in diverse *Vibrio* species including *V.*

221 *parahaemolyticus, V. diabolicus, V. antiquarius, V. campbelli* and *V. alginolyticus* (Fig. S4).

222 Interestingly, the 5 genomes containing *vopQ* but lacking *vopS* belonged to two *Vibrio* species,

223 *V. harveyi* and *V. tubiashii*.

224

225 *VopQ-induced pro-survival signaling is independent of endosomal deacidification*

226 Next, we wanted to understand how VopQ could activate ERK1/2 MAPK signaling in the host.

227 The VopQ channel de-acidifies vacuolar and lysosomal compartments, but also inhibits

228 homotypic fusion of yeast vacuoles, a model for Rab GTPase- and SNARE-dependent fusion

10

229   between the lysosome and autophagosome (*9, 20*). Mutation of serine 200 to a proline creates a

230   mutant, VopQ^{S200P}, that is still able to neutralize the vacuole or lysosome, but can no longer

231   block fusion (*9*). This observation is likely due to reduced binding of VopQ^{S200P} to the V-

232   ATPase (*16*). To test if VopQ's activation of ERK1/2 MAPK signaling was caused by one or

233   both of these functions, we exchanged the chromosomal copy of the *vopQ* gene in the *V. para*

234   T3SS1$^+$ strain with a version encoding VopQ^{S200P} creating the *V. para* T3SS1$^+$*vopQ*^{S200P} strain.

235   We tested the cytotoxicity of this strain during MEF infection and found that the VopQ^{S200P}

236   mutant was no less lethal than wild-type VopQ (Fig. S3A). However, unlike its parent strain, *V.*

237   *para* T3SS1$^+$*vopQ*^{S200P} was unable to induce ERK1/2 phosphorylation and downstream

238   production of Egr1 in MEFs (Fig. 2E,F). Notably, treatment of MEFs with chloroquine, a drug

239   that prevents lysosomal acidification, is not able to induce phosphorylation of ERK1/2 (Fig. 2E).

240   These data suggest ERK1/2 MAPK signaling is not activated by lysosomal deacidification alone

241   and is instead dependent on VopQ's strong physical interaction with the V-ATPase. We

242   therefore propose two models by which VopQ could induce ERK1/2 MAPK signaling. In the

243   first, VopQ's inhibition of lysosome-autophagosome fusion directly activates ERK1/2 MAPK

244   signaling. In the second, VopQ manipulates another pathway upstream of both lysosome-

245   autophagosome fusion and ERK1/2, thereby altering these two pathways in parallel.

246

247   *VopQ-induced pro-survival ERK1/2 signaling is dependent on IRE1*

248   To test these models, we aimed to identify a signaling pathway that could be upstream of both

249   autophagosome-lysosome fusion and ERK1/2 MAPK signaling. The unfolded protein response

250   has previously been linked to both of these processes through IRE1's connections to the UPR

251   and the ERAD pathway (*21-24*). Moreover, induction of ER stress with a proline analogue was

11

252   previously shown to partially stimulate IRE1-dependent ERK1/2 activation to promote cell

253   survival by an undefined mechanism (*25*). To examine if the UPR played a role, we tested if

254   VopQ's activation of ERK1/2 and downstream EGR1 production was dependent on any of the

255   three branches of UPR: IRE1, ATF6, or PERK(*26*). We infected *IRE1*^{-/-} MEFs, *Atf6*^{-/-} MEFs,

256   *PERK*^{-/-} MEFs and wild-type MEFs with *V. para* T3SS1[+] and *V. para* T3SS1[-] and monitored

257   phosphorylation of ERK1/2 and accumulation of Egr1 by Western blot. While infection of *Atf6*^{-/-}

258   MEFs, *PERK*^{-/-} MEFs, and wild-type MEFs with *V. para* T3SS1[+] resulted in robust ERK1/2

259   phosphorylation 45 and 60 minutes post-infection, phosphorylated ERK1/2 was not detected in

260   *IRE1*^{-/-} MEFs infected with *V. para* T3SS1[+] (Fig. 3A,B). Consistent with this observation,

261   accumulation of Egr1 was also not observed in *IRE1*^{-/-} MEFs infected with *V. para* T3SS1[+] (Fig.

262   3A). VopQ was still cytotoxic to *IRE1*^{-/-} MEFs (Fig. S5A), consistent with the maintained

263   cytotoxicity of VopQ[S200P] in wild-type MEFs despite its inability to activate ERK1/2 (Fig. S3A).

264   These data suggest that VopQ induces ERK1/2 phosphorylation by an IRE1-dependent

265   mechanism.

266   VopQ-mediated cytotoxicity was also conserved in the *Atf6*^{-/-} and *PERK*^{-/-} MEFs (Fig. S5B,C).

267   Both the *Atf6*^{-/-} and *PERK*^{-/-} cell lines exhibited the same pattern of ERK1/2 phosphorylation and

268   Egr1 accumulation upon T3SS1[+] infection as wild-type MEFs (Fig. 3B), indicating that VopQ's

269   activation of ERK1/2 was specifically IRE1-dependent. Finally, we stimulated wild-type, *IRE1*^{-/-}*,*

270   *Atf6*^{-/-} and *PERK*^{-/-} MEFs with fetal bovine serum (FBS) to assess whether the well described

271   growth factor-stimulated ERK1/2 MAPK signaling was functional in these cell lines (*27*). FBS-

272   stimulated ERK1/2 phosphorylation and downstream Egr1 expression was observed in all cell

273   lines (Fig. 3C). These data strongly support our model that VopQ's IRE1-dependent activation of

274   ERK1/2 occurs through pathway that is separate from the established growth factor-stimulated

275   pathway mediated by Ras and Raf (*27*).

276

277   *VopQ expression results in IRE1 activation in yeast*

278   Next we asked if VopQ activates IRE1. VopQ toxicity is dependent on the assembly c subunit of

279   the V_o V-ATPase in yeast independent of the vacuolar localization of the complex. This led us

280   led us to hypothesize that interaction of VopQ and the c subunit ring could also take place in the

281   endoplasmic reticulum (ER) where the V_o complex initially forms (*16*). In addition, the ER is the

282   source of membranes for autophagosomes, thus a block in autophagic flux may also perturb the

283   protein to lipid ratio of the ER (*28*). We predicted that if either of these scenarios occurred, the

284   membrane perturbations caused by VopQ may activate the UPR, which is mediated by IRE1 in

285   yeast, either through the disruption of the ER lumen environment or through the activation of

286   lipid bilayer stress (*29-32*). IRE1 is a type I ER-resident transmembrane protein that contains a

287   protein kinase and an endoribonuclease domain in its cytoplasmic region (*33*). IRE1 also

288   contains an amphipathic helix which can sense perturbations in the lipid bilayer, leading to

289   activation and initiation of the UPR (*30*).

290   To test this hypothesis, we assessed the clustering of IRE1 in yeast by visualizing endogenously

291   expressed IRE1p-GFP (20). Plasmids carrying galactose-inducible genes encoding wild type

292   VopQ, a V-ATPase binding mutant VopQ[S200P], and VopA were transformed into the BY4741

293   IRE1-GFP yeast strain. VopA is a *V. para* T3SS2 effector that kills yeast by a mechanism that is

294   distinct from VopQ and was included as a control (*34*). Upon galactose induction serial growth

295   assays showed that VopQ and VopA both inhibited growth in the BY4741 IRE1-GFP strain

296   while VopQ[S200P] and vector alone control did not (Fig. S6). We then monitored IRE1p-GFP

13

297   clustering, or foci formation, at 30 and 45 minutes post galactose induction by confocal

298   microscopy. Treatment with dithiothreitol (DTT) for the same period was used as a positive

299   control for UPR stress. Yeast expressing VopQ, but not VopQ^{S200P} or VopA induced IRE1p-GFP

300   foci formation (Fig. 3D). IRE1p-GFP foci formation was observed, on average, in about 70% of

301   DTT treated cells compared to about 15% in cells expressing VopQ (Fig. 3E). This difference

302   was expected because DTT treatment is homogeneous, whereas expression of VopQ is stochastic

303   (*35*). Our data indicate that expression of VopQ in yeast results in IRE1 activation.

304

305   *VopQ causes induction of the IRE1 branch of the UPR of mammalian cells during infection*

306   We next asked if VopQ also activates IRE1 in mammalian cells during infection. IRE1 is

307   normally sequestered by BiP, but is released upon UPR activation when it then oligomerizes,

308   *trans*-autophosphorylates and activates its endoribonuclease activity, resulting in the non-

309   conventional splicing of XBP1 mRNA in mammalian cells (*36-38*). To determine if the IRE1

310   branch of the UPR was activated by VopQ in early infection time points, we measured levels of

311   phospho-IRE1α in MEFs by Western blot at 45 and 60 minutes post infection. Our results

312   indicate that *V. para* T3SS1^{+} induces IRE1α phosphorylation in a VopQ-dependent manner (Fig.

313   3F) and that T3SS1^{+}*vopQ*^{S200P} is not able to induce IRE1α phosphorylation. Taken together,

314   these data indicate that the V-ATPase binding activity of VopQ activates the IRE1 branch of the

315   UPR in both MEFs and yeast.

316

317   *VopQ-induced pro-survival ERK signaling is dependent on IRE1 kinase activity*

318   Next, we wanted to further determine if the catalytic activities of IRE1 are required for VopQ-

319   induced ERK1/2 signaling. IRE1 contains both protein kinase and an endoribonuclease domain

14

320   in its cytoplasmic region (*33*). To test if the kinase or endonuclease activity of IRE1 is required

321   for ERK signaling, MEFs were treated before *V. para* infection with KIRA6 or 4μ8c, an IRE1

322   specific kinase inhibitor and a potent inhibitor of IRE1 RNase activity, respectively (Fig. 4A).

323   Strikingly, ERK1/2 phosphorylation and Egr1 protein expression were not observed in infected

324   MEFs treated with the kinase inhibitor KIRA6. However, 4μ8c treatment appeared to have no

325   effect on VopQ-induced ERK1/2 phosphorylation and Egr1 protein expression. Taken together,

326   this data indicates that the pro-survival ERK signaling induced by VopQ during *V. para* infection

327   is dependent on IRE1 kinase activity.

328

Discussion

329

330   By studying the function of two effectors of the T3SS1 of the seafood-borne pathogen *V. para*,

331   we have shown that T3SS effectors act together to systematically manipulate the host response.

332   We observe that the effector VopQ is responsible for the T3SS1-mediated activation of cell

333   survival and repression of cell death networks and another effector VopS is responsible for

334   dampening this response. Of note, VopS has been established to AMPylate and thereby

335   inactivate Rac, a known activator of MEK1/2 mediated ERK signaling(*17*). Furthermore, in

336   *Vibrio alginolytcus*, a *Vibrio* species closely related to *V. para,* VopS was found to be required

337   for the rapid induction of apoptosis in infected cells (*39*). The association of VopQ with the V-

338   ATPase elicits early activation of ERK1/2 phosphorylation that is turned off by the delayed

339   temporal action of VopS (Fig. 4B).

340   Manipulation of the V-ATPase to affect signaling in the cell has been previously observed with

341   oncogenic Ras, which induces a Rac-dependent plasma membrane ruffling and micropinocytosis.

342   However, in the case of oncogenic Ras, activation of Rac is dependent on the activity of the V-

15

343   ATPase along with its relocation to the plasma membrane (*40*). Importantly, the activation

344   ERK1/2 MAPK signaling by VopQ does not occur through the growth factor inducible Ras-

345   mediated pathway, but instead is dependent on the kinase activity of the ER stress sensor and

346   cell-fate executor, IRE1 (Fig. 4B). Activation of ERK1/2 MAPK signaling specifically through

347   the IRE1-branch of the UPR by a bacterial effector has not previously been reported.

348   The evolutionary conservation of *vopQ* and *vopS* in *Vibrio* species retaining synteny in the

349   T3SS1 neighborhood suggests that their concerted function is important for proper modulation of

350   the host response. Effector pairs with opposing effects yet synergistic effects during infection are

351   not unknown. YopJ and YopM of *Yersinia pestis* were previously described as having opposing

352   effects on Interleukin signaling and caspase-1 processing which synergistically suppressed pro-

353   inflammatory cytokines during infection (*41*). In *Salmonella*, the effectors SptP and SopE act as

354   respective GTP activating proteins (GAPs) and Guanine nucleotide exchange factors (GEFs) for

355   Cdc42 and Rac. Rapid degradation of SopE allows for the temporal regulation of Cdc42 and Rac

356   activity during *Salmonella* infection (*42*). Furthermore, *Legionella pneumonphila* utilizes several

357   such pairs of effectors such as SidM/DrrA and LepB, SidH and LubX, and AnkX and Lem3 (*43-*

358   *49*). Together these effector pairs coordinate the establishment, maintenance and properly timed

359   escape from the LCV environmental niche *Legionella* requires to replicate (*50, 51*).

360   The targeting of autophagy, UPR and MAPK signaling together is not unprecedented for

361   pathogens. For example, the mycotoxin Patulin was found to manipulate these pathways though

362   the inhibition of cathepsin B and cathepsin D, which leads to an accumulation of p62. Increased

363   p62-mediated autophagy activates the PERK and IRE1 branches of the UPR through increased

364   reactive oxygen species production. UPR activation then results in activation of ERK1/2 and

365   phosphorylation of BAD, resulting in increased survival of host cells (*52*). Several viruses rely

16

366   on the interplay of UPR and MAPK signaling for virulence as well. Dengue virus (DENV) relies

367   on UPR activation of JNK signaling to induce autophagy and increase viral load of infected cells.

368   Treatment with a JNK inhibitor decreased viral titers and reduced symptoms of DENV2 in mice

369   (*53*). Recently the coronavirus infectious bronchitis virus (IBV) was found to rely on the

370   activation of IRE1 and ERK1/2, but not XBP1 or JNK, for the induction of autophagic flux and

371   pro-survival signaling during IBV infection (*54*).

372   We and others have observed that the ERK1/2 MAPK signaling can be regulated either directly

373   or indirectly through the IRE1 branch of the UPR. However, it remains unclear if VopQ's

374   induction of IRE1 signaling is caused by the manipulation of autophagy or via localized

375   perturbations in the ER membrane caused by VopQ's interaction with assembly intermediates of

376   the V-ATPase V_o subcomplex in the ER. Deciphering the epistatic relationship between VopQ's

377   association with the V-ATPase and activation of IRE1 will be the subject of future studies that

378   will be important in understanding the role of the V-ATPase-UPR-MAPK feedback network in

379   both cellular homeostasis and bacterial infection. Similarly, the interaction of VopQ with the V-

380   ATPase at the ER should be further studied to determine if this interaction is sufficient to

381   activate IRE1's lipid bilayer stress response and ERK1/2 MAPK signaling independently of

382   autophagy (*31, 55*). Other groups have hypothesized that Ire1's interaction with the adapter

383   protein Nck plays an important role in activation of ERK1/2 signaling upon ER stress; however,

384   whether IRE1's kinase or endonuclease activity are needed was unknown (*25*). Our studies

385   indicate that the kinase activity of IRE1 is required, but the mechanism by which IRE1 kinase

386   activity leads to ERK1/2 MAPK signaling is still poorly understood. Future experiments to

387   dissect the role of Nck and Rho GTPase activation in this process would be a valuable addition

17

388   to understanding this molecular mechanism of IRE1 induced, growth factor independent ERK1/2

389   MAPK signaling.

390

391   **Materials and Methods**

392   *Bacterial strains and culture conditions*

393   The *Vibrio parahaemolyticus* POR3 (POR1Δ*vcrD2*) and POR4 (POR1Δ*vcrD1*/*vcrD2*) strains

394   were generously provided by Drs. Tetsuya Iida and Takeshi Honda of Osaka University. *Vibrio*

395   strains were cultured at 30°C in MLB (Luria-Bertani broth +3% NaCl).All *V. para* strains except

396   *V. para* T3SS1$^+$*vopQ*^{S200P} were from previous studies (Table S1). The T3SS1$^+$*vopQ*^{S200P} strain

397   was created by cloning the *vopQ*^{S200P} allele (*9*) flanked by the nucleotide sequences 1 kb

398   upstream and 1 kb downstream of vopQ (vp1680) into pDM4, a Cm^{R}OriR6K suicide plasmid. *E.*

399   *coli* S17 (λ pir) was used to conjugate the resulting plasmid into the POR3 strain and

400   transconjugants were selected on media containing 25mg/ml chloramphenicol. Bacteria were

401   then counter-selected on 15% sucrose and insertion of the *vopQ*^{S200P} allele was confirmed by

402   PCR.

403

404   *Mammalian Cell Culture*

405   Primary Adult Dermal Fibroblasts ATCC® PCS-201-01 (PHDFs) were purchased from ATCC

406   and revived and maintained at 5% CO_2 and 37°C in Low Serum Primary Fibroblast Media

407   (ATCC) according to ATCC instructions. Wild-type Mouse Embryonic Fibroblasts (MEFs) were

408   gift of Dr. Jenna Jewell and *IRE1*$^{-/-}$, *PERK*$^{-/-}$ and *Atf6*$^{-/-}$ MEFs were kindly provided by Dr.

409   Fumiko Urano. MEFs were maintained at 5% CO_2 and 37°C in high-glucose Dulbecco's

18

410   modified Eagle's medium (DMEM, Gibco) supplemented with 10% (v/v) fetal bovine serum

411   (Sigma-Aldrich), 1% (v/v) penicillin-streptomycin-glutamine, and 1% (v/v) sodium pyruvate.

412

413   *Yeast strains and plasmids*

414   All yeast genetic techniques were performed by standard procedures described previously (*56*).

415   All strains were cultured in either rich (YPD: 1% yeast extract, 2% peptone, and 2% dextrose) or

416   complete synthetic minimal (CSM) media (Sigma) lacking appropriate amino acids with 2%

417   dextrose, 2% raffinose, or 2% galactose. Yeast were serially diluted and spotted onto agar plates

418   to assay fitness and temperature sensitivity per standard technique. Yeast strains used in this

419   study were BY4741 (MATa *his3Δ0 leu2Δ0 met15Δ0 ura3Δ0*) and BY4741 IRE1-GFP (MATa

420   *his3Δ0 leu2Δ0 met15Δ0 ura3Δ0 IRE1-GFP*) (Thermo Fisher) as indicated.

421   Plasmids pRS416-Gal1-FLAG-VopQ and pRS416-Gal1-FLAG-VopQ^{S200P} were generated by

422   sub-cloning pRS413-Gal1-VopQ and pRS413-Gal1-VopQ^{S200P} (previously published (*9*)) into

423   the *BamHI* and *EcoRV* sites of pRS416-Gal1. Plasmid pRS416-Gal1-VopA-FLAG was

424   generated by sub-cloning pRS413-Gal1-VopA-FLAG (previously published (*34*)) into the *EcoRI*

425   and *XhoI* sites of pRS416-Gal1.

426

427   *Infection of PHDFs for RNA-sequencing and quantitative RT-PCR*

428   For RNA-sequencing, PHDFs were seeded onto 6-well plates at a density of $1x10^5$ cells/mL and

429   grown for 18-20 hours to ~80% confluency. Overnight *V. para* cultures were normalized to an

430   OD_{600} = 0.2 and sub-cultured to OD_{600} = 0.6. Bacteria were pelleted, resuspended in un-

431   supplemented DMEM and grown at 37°C for 45 minutes to pre-induce T3SS1 expression (*14*).

432   PHDFs were washed with un-supplemented DMEM and then infected with pre-induced *V. para*

433   strains at a multiplicity of infection (MOI) of 10. Plates were centrifuged at 1000xg for 5 minutes

434   to synchronize infection and incubated at 37°C, 5% CO_2. At 90 minutes post-infection,

435   RNAprotect Cell Reagent (Qiagen) was added to stop the infection and preserve the RNA. Cells

436   were harvested by scraping, pooled and pellets were resuspended in RLT-plus buffer (Qiagen)

437   and stored at -80°C. The same infection protocol was followed for qPCR experiments with

438   PHDFs and MEFs. For MEK1/2 inhibition qPCR experiments MEFs were incubated with 10μM

439   U0126 (Cell Signaling) or 10μM DMSO (vehicle) during and for one hour prior to infection.

440

441   *RNA Isolation and RNA-sequencing*

442   RNA isolation was performed the same for PHDFs and MEFs. Cells were lysed with $27G^{1/2}$

443   needles and then homogenized with QiAshredder columns (Qiagen). Total RNA from triplicate

444   experiments were purified with the RNAeasy Plus Kit (Qiagen). Quality of purified total RNA

445   samples was determined by Agilent 2100 Bioanalyzer and only samples with RIN score 9 or

446   higher were used. RNA concentration was measured by Qubit fluorimeter prior to library

447   prep. 4μg of total DNAse treated RNA was run through the TruSeq Stranded Total RNA LT

448   Sample Prep Kit from Illumina as previously described(*3*). Samples were quantified by Qubit

449   before being normalized, pooled, and then sequenced on the Illumina Hiseq 2500 with SBS v3

450   reagents. Each sample was sequenced at a depth of at least 25 million 50-nucleotide single-end

451   reads.

452

453   *Infection of MEFs for Immunoblotting*

454   For ERK1/2 and Egr1 immunoblotting experiments, MEFs were starved in un-supplemented

455   DMEM for one hour prior to infection/treatment to remove background growth factor-stimulated

20

456   MAPK signaling. MEFs were not starved for in phospho-IRE1α experiments in order to prevent

457   background activation of the UPR by nutritional stress. Cells were then infected at an MOI = 10

458   with *V. para* as described above or with treated DMEM supplemented with 10% (v/v) fetal

459   bovine serum (FBS, Sigma-Aldrich). To inhibit IRE1 nuclease and kinase activity, cells were

460   treated with 100μM 4μ8c for 24hrs and 100μM KIRA6 for 1hr before infection, respectively.

461

462   *Immunoblotting*

463   MEFs were infected as described above and washed with 1X ice-cold PBS and collected by

464   scraping at each timepoint. Collected cells were pelleted (1,000xg) and washed twice in ice-cold

465   1X PBS and lysed in RIPA buffer (50mM Tris, pH 8.0, 150mM NaCl, 5mM EDTA, 1% Nonidet

466   P-40, 0.5% sodium deoxycholate, 0.1% SDS) with protease and phosphatase inhibitors (Roche

467   Applied Science) for 20 minutes on ice. Total protein concentration of lysed supernatants was

468   determined by Bradford assay and all samples were normalized for total protein prior to gel

469   electrophoresis and immunoblotting. Total ERK1/2 and Phospho-ERK1/2 were detected with

470   Cell Signaling Technologies (CST) p44/42 MAPK (137F5) and P-p44/42 MAPK T202/Y204

471   (197G2) primary antibodies, respectively. EGR1 was detected using CST EGR1 (15F7) and β-

472   actin was detected by Sigma-Aldrich A2228 Monoclonal Anti-β-actin. Total IRE1α and

473   Phospho-IRE1α were detected by CST IRE1α (14C10) and Novus IRE1α (pSer724),

474   respectively. α-tubulin was detected by Santa Cruz α-tubulin (B-7). Secondary HRP-conjugated

475   antibodies used were donkey anti-rabbit (GE Healthcare) and goat anti-mouse (Sigma-Aldrich).

476

477   *IRE1p-GFP Clustering assay*

21

478   Yeast strains were grown to mid-log phase (OD_{600} ~0.5) in CSM media lacking uracil with 2%

479   raffinose. Cultures were then treated with 2% galactose, 2% raffinose, or 2% raffinose + 5mM

480   DTT for 30 or 45 minutes. Cultures were collected, resuspended in 1X PBS, and fixed with 4%

481   paraformaldehyde. Confocal images were acquired using a Zeiss LSM800 with Zen software.

482   Images were processed with ImageJ (National Institutes of Health) and Adobe Photoshop CS6.

483   For quantification, the presence of IRE1-GFP foci was scored in 100 cells per experiment over

484   three independent experiments.

485

486   *Statistical Methods*

487   For RNA-sequencing DE analysis statistical cutoffs were as follows: false discovery rate

488   (FDR) ≤ 0.01, $\log_2$counts-per-million ($\log_2$CPM) ≥ 0 and the absolute value of fold change (FC)

489   ≥ 1.5. For IPA pathway and biological network analysis the *p* values are presented as -

490   log(Pvalue) and the cutoff for significance was $p < 0.05$. FDRs and *p* values are reported in

491   Tables S2-6. For quantitative RT-PCR *p* values were calculated by one-way ANOVA and

492   Dunnett's multiple comparisons test. For the quantification of IRE1-GFP clustering *p* values

493   were calculated by Student's unpaired t-test (two-tailed).

494

495   Additional Materials and methods are available as supplementary materials

496

497   **Supplementary Materials**

498   Materials and Methods

499   **Fig. S1**. Rapid cytotoxicity of *V. para* T3SS1 is dependent on the effector VopQ.

500   **Fig. S2**. Analysis of RNA sequencing data and RT-qPCR verification.

22

501   **Fig. S3**. Conservation of T3SS1 VopQ-dependent cytotoxicity and MEK1/2 dependent EGR1

502   expression in MEFs.

503   **Fig. S4.** Co-occurrence of *vopQ* and *vopS* in *Vibrio* strains with T3SS1 synteny.

504   **Fig. S5**. VopQ-mediated cytotoxicity is conserved in UPR mutant cell lines.

505   **Fig. S6.** VopQ but not VopQ^{S200P} inhibits growth of BY471 IRE1-GFP yeast.

506   **Table S1**. Bacterial strains used in this work.

507   **Table S2.** Complete RNA sequencing Differential Expression Data.

508   **Table S3.** Differential Expression of T3SS1-specific genes.

509   **Table S4.** IPA Canonical Pathway Analysis of Differential Expression Data.

510   **Table S5.** IPA Network (Disease and Biofunction) Analysis of Differential Expression Data.

511   **Table S6.** Expression of alternate MAPK pathway target genes

512   **Table S7.** SyntTax VopQ and VopS cooccurence in Vibrio genomes with T3SS1 Synteny.

513

514   **References and Notes:**

515 1.   N. M. Alto, K. Orth, Subversion of cell signaling by pathogens. *Cold Spring Harb Perspect*
516   *Biol* **4**, a006114 (2012).
517 2.   D. L. Burdette, M. L. Yarbrough, A. Orvedahl, C. J. Gilpin, K. Orth, Vibrio
518   parahaemolyticus orchestrates a multifaceted host cell infection by induction of
519   autophagy, cell rounding, and then cell lysis. *Proc Natl Acad Sci U S A* **105**, 12497-12502
520   (2008).
521 3.   N. J. De Nisco, M. Kanchwala, P. Li, J. Fernandez, C. Xing, K. Orth, The cytotoxic type 3
522   secretion system 1 of Vibrio rewires host gene expression to subvert cell death and
523   activate cell survival pathways. *Sci Signal* **10**, (2017).
524 4.   K. Makino, K. Oshima, K. Kurokawa, K. Yokoyama, T. Uda, K. Tagomori, Y. Iijima, M.
525   Najima, M. Nakano, A. Yamashita, Y. Kubota, S. Kimura, T. Yasunaga, T. Honda, H.
526   Shinagawa, M. Hattori, T. Iida, Genome sequence of Vibrio parahaemolyticus: a
527   pathogenic mechanism distinct from that of V cholerae. *The Lancet* **361**, 743-749 (2003).
528 5.   M. de Souza Santos, K. Orth, Intracellular Vibrio parahaemolyticus escapes the vacuole
529   and establishes a replicative niche in the cytosol of epithelial cells. *mBio* **5**, e01506-
530   01514 (2014).

531 6.   K. S. Park, T. Ono, M. Rokuda, M. H. Jang, K. Okada, T. Iida, T. Honda, Functional
532   characterization of two type III secretion systems of Vibrio parahaemolyticus. *Infect*
533   *Immun* **72**, 6659-6665 (2004).
534 7.   N. O'Boyle, A. Boyd, Manipulation of intestinal epithelial cell function by the cell
535   contact-dependent type III secretion systems of Vibrio parahaemolyticus. *Front Cell*
536   *Infect Microbiol* **3**, 114 (2014).
537 8.   T. Ono, K. S. Park, M. Ueta, T. Iida, T. Honda, Identification of proteins secreted via
538   Vibrio parahaemolyticus type III secretion system 1. *Infect Immun* **74**, 1032-1042 (2006).
539 9.   A. Sreelatha, T. L. Bennett, E. M. Carpinone, K. M. O'Brien, K. D. Jordan, D. L. Burdette, K.
540   Orth, V. J. Starai, Vibrio effector protein VopQ inhibits fusion of V-ATPase-containing
541   membranes. *Proc Natl Acad Sci U S A* **112**, 100-105 (2015).
542 10.   M. L. Yarbrough, Y. Li, L. N. Kinch, N. V. Grishin, H. L. Ball, K. Orth, AMPylation of Rho
543   GTPases by Vibrio VopS disrupts effector binding and downstream signaling. *Science*
544   **323**, 269-272 (2009).
545 11.   D. Salomon, Y. Guo, L. N. Kinch, N. V. Grishin, K. H. Gardner, K. Orth, Effectors of animal
546   and plant pathogens use a common domain to bind host phosphoinositides. *Nat*
547   *Commun* **4**, 2973 (2013).
548 12.   A. Sreelatha, K. Orth, V. J. Starai, The pore-forming bacterial effector, VopQ, halts
549   autophagic turnover. *Autophagy* **9**, 2169-2170 (2013).
550 13.   D. L. Burdette, J. Seemann, K. Orth, Vibrio VopQ induces PI3-kinase-independent
551   autophagy and antagonizes phagocytosis. *Mol Microbiol* **73**, 639-649 (2009).
552 14.   C. A. Broberg, L. Zhang, H. Gonzalez, M. A. Laskowski-Arce, K. Orth, A Vibrio effector
553   protein is an inositol phosphatase and disrupts host cell membrane integrity. *Science*
554   **329**, 1660-1662 (2010).
555 15.   A. R. Woolery, X. Yu, J. LaBaer, K. Orth, AMPylation of Rho GTPases subverts multiple
556   host signaling processes. *J Biol Chem* **289**, 32977-32988 (2014).
557 16.   W. Peng, A. K. Casey, J. Fernandez, K. Servage, Z. Chen, Y. Li, D. R. Tomchick, K. Orth, A
558   distinct inhibitory mechanism of the V-ATPase by Vibrio VopQ revealed by cryo-EM. *Nat*
559   *Struct Mol Biol*, (2020).
560 17.   M. L. Yarbrough, Y. Li, L. N. Kinch, N. V. Grishin, H. L. Ball, K. Orth, AMPylation of Rho
561   GTPases by Vibrio VopS Disrupts Effector Binding and Downstream Signaling. *Science*
562   **323**, 269-272 (2009).
563 18.   C. Hodge, J. Liao, M. Stofega, K. Guan, C. Carter-Su, J. Schwartz, Growth hormone
564   stimulates phosphorylation and activation of elk-1 and expression of c-fos, egr-1, and
565   junB through activation of extracellular signal-regulated kinases 1 and 2. *J Biol Chem*
566   **273**, 31327-31336 (1998).
567 19.   T. Shimohata, M. Nakano, X. Lian, T. Shigeyama, H. Iba, A. Hamamoto, M. Yoshida, N.
568   Harada, H. Yamamoto, M. Yamato, K. Mawatari, T. Tamaki, Y. Nakaya, A. Takahashi,
569   Vibrio parahaemolyticus infection induces modulation of IL-8 secretion through dual
570   pathway via VP1680 in Caco-2 cells. *J Infect Dis* **203**, 537-544 (2011).
571 20.   S. Nakamura, T. Yoshimori, New insights into autophagosome-lysosome fusion. *J Cell Sci*
572   **130**, 1209-1216 (2017).

573 21. M. M. Yan, J. D. Ni, D. Song, M. Ding, J. Huang, Interplay between unfolded protein
574   response and autophagy promotes tumor drug resistance. *Oncol Lett* **10**, 1959-1969
575   (2015).

576 22. H. O. Rashid, R. K. Yadav, H. R. Kim, H. J. Chae, ER stress: Autophagy induction, inhibition
577   and selection. *Autophagy* **11**, 1956-1977 (2015).

578 23. N. J. Darling, S. J. Cook, The role of MAPK signalling pathways in the response to
579   endoplasmic reticulum stress. *Biochim Biophys Acta* **1843**, 2150-2163 (2014).

580 24. X. Cheng, H. Liu, C. C. Jiang, L. Fang, C. Chen, X. D. Zhang, Z. W. Jiang, Connecting
581   endoplasmic reticulum stress to autophagy through IRE1/JNK/beclin-1 in breast cancer
582   cells. *Int J Mol Med* **34**, 772-781 (2014).

583 25. D. T. Nguyen, S. Kebache, A. Fazel, H. N. Wong, S. Jenna, A. Emadali, E. H. Lee, J. J.
584   Bergeron, R. J. Kaufman, L. Larose, E. Chevet, Nck-dependent activation of extracellular
585   signal-regulated kinase-1 and regulation of cell survival during endoplasmic reticulum
586   stress. *Mol Biol Cell* **15**, 4248-4260 (2004).

587 26. M. Schroder, R. J. Kaufman, The mammalian unfolded protein response. *Annu Rev*
588   *Biochem* **74**, 739-789 (2005).

589 27. M. Katz, I. Amit, Y. Yarden, Regulation of MAPKs by growth factors and receptor tyrosine
590   kinases. *Biochim Biophys Acta* **1773**, 1161-1176 (2007).

591 28. S. Davis, J. Wang, S. Ferro-Novick, Crosstalk between the Secretory and Autophagy
592   Pathways Regulates Autophagosome Formation. *Dev Cell* **41**, 23-32 (2017).

593 29. N. S. Hou, A. Gutschmidt, D. Y. Choi, K. Pather, X. Shi, J. L. Watts, T. Hoppe, S. Taubert,
594   Activation of the endoplasmic reticulum unfolded protein response by lipid
595   disequilibrium without disturbed proteostasis in vivo. *Proc Natl Acad Sci U S A* **111**,
596   E2271-2280 (2014).

597 30. K. Halbleib, K. Pesek, R. Covino, H. F. Hofbauer, D. Wunnicke, I. Hanelt, G. Hummer, R.
598   Ernst, Activation of the Unfolded Protein Response by Lipid Bilayer Stress. *Mol Cell* **67**,
599   673-684 e678 (2017).

600 31. R. Volmer, K. van der Ploeg, D. Ron, Membrane lipid saturation activates endoplasmic
601   reticulum unfolded protein response transducers through their transmembrane
602   domains. *Proc Natl Acad Sci U S A* **110**, 4628-4633 (2013).

603 32. R. Covino, G. Hummer, R. Ernst, Integrated Functions of Membrane Property Sensors
604   and a Hidden Side of the Unfolded Protein Response. *Mol Cell* **71**, 458-467 (2018).

605 33. W. Tirasophon, A. A. Welihinda, R. J. Kaufman, A stress response pathway from the
606   endoplasmic reticulum to the nucleus requires a novel bifunctional protein
607   kinase/endoribonuclease (Ire1p) in mammalian cells. *Genes Dev* **12**, 1812-1824 (1998).

608 34. J. E. Trosky, S. Mukherjee, D. L. Burdette, M. Roberts, L. McCarter, R. M. Siegel, K. Orth,
609   Inhibition of MAPK signaling pathways by VopA from Vibrio parahaemolyticus. *J Biol*
610   *Chem* **279**, 51953-51957 (2004).

611 35. A. Raj, A. van Oudenaarden, Nature, nurture, or chance: stochastic gene expression and
612   its consequences. *Cell* **135**, 216-226 (2008).

613 36. Y. Kimata, Y. Ishiwata-Kimata, T. Ito, A. Hirata, T. Suzuki, D. Oikawa, M. Takeuchi, K.
614   Kohno, Two regulatory steps of ER-stress sensor Ire1 involving its cluster formation and
615   interaction with unfolded proteins. *J Cell Biol* **179**, 75-86 (2007).

25

616 37. A. Bertolotti, Y. Zhang, L. M. Hendershot, H. P. Harding, D. Ron, Dynamic interaction of
617   BiP and ER stress transducers in the unfolded-protein response. *Nat Cell Biol* **2**, 326-332
618   (2000).
619 38. S. H. Back, M. Schroder, K. Lee, K. Zhang, R. J. Kaufman, ER stress signaling by regulated
620   splicing: IRE1/HAC1/XBP1. *Methods* **35**, 395-416 (2005).
621 39. Z. Zhao, J. Liu, D. Y., W. Huang, C. Ren, D. R. Call, C. Hu, The Vibrio alginolyticus T3SS
622   effectors, Val1686 and Val1680, induce cell rounding, apoptosis and lysis of fish
623   epithelial cells. *Virulence* **9**, 318-330 (2018).
624 40. C. Ramirez, A. D. Hauser, E. A. Vucic, D. Bar-Sagi, Plasma membrane V-ATPase controls
625   oncogenic RAS-induced macropinocytosis. *Nature* **576**, (2018).
626 41. D. Ratner, M. Pontus, A. Ornig, K. K. Starheim, R. Marty-Roix, M. K. Proulx, J. D. Goguen,
627   E. Lien, Manipulation of Interleukin-1β and Interleukin-18 Production by Yersinia pestis
628   Effectors YopJ and YopM and Redundant Impact on Virulence. *Journal of Biological
629   Chemistry* **291**, 9894–9905 (2016).
630 42. J. C. Patel, J. E. Galan, Manipulation of the host actin cytoskeleton by Salmonella — all in
631   the name of entry. *Curr Opin Microbiol* **8**, 10-15 (2005).
632 43. M. P. Müller, H. Peters, J. Blümer, W. Blankenfeldt, R. S. Goody, A. Itzen, The Legionella
633   Effector Protein DrrA AMPylates the Membrane Traffic Regulator Rab1b. *Science* **329**,
634   946-949 (2010).
635 44. M. R. Neunuebel, Y. Chen, A. H. Gaspar, P. S. Backlund, A. Yergey, M. P. Machner, De-
636   AMPylation of the Small GTPase Rab1 by the Pathogen Legionella pneumophila. *Science*
637   **333**, 453-456 (2011).
638 45. S. Mukherjee, X. Liu, K. Arasaki, J. McDonough, J. E. Galan, C. R. Roy, Modulation of Rab
639   GTPase Function by a Protein Phosphocholine Transferase. *Nature* **477**, 103-106 (2011).
640 46. V. Campanacci, S. Mukherjee, C. R. Roy, J. Cherfils, Structure of the Legionella Effector
641   AnkX Reveals the Mechanism of Phosphocholine Transfer by the FIC Domain. *EMBO J.*
642   **32**, 1469-1477 (2013).
643 47. E. A. Creasey, R. R. Isberg, The protein SdhA maintains the integrity of the Legionella-
644   containing vacuole. *Proc Natl Acad Sci U S A* **109**, 3481-3486 (2012).
645 48. R. K. Laguna, E. A. Creasey, Z. Li, N. Valtz, R. R. Isberg, A Legionella pneumophila-
646   translocated substrate that is required for growth within macrophages and protection
647   from host cell death *Proc Natl Acad Sci U S A* **103**, 18745-18750 (2006).
648 49. Y. Tan, R. J. Arnold, Z. Q. Luo, Legionella pneumophila regulates the small GTPase Rab1
649   activity by reversible phosphorylcholination. *Proc Natl Acad Sci U S A* **108**, 21212-21217
650   (2011).
651 50. R. R. Isberg, T. O'conner, M. Heidtman, The Legionella pneumophila Replication Vacuole:
652   Making a Cozy Niche Inside Host Cells. *Nat. Rev. Microbiol.* **7**, 13-24 (2009).
653 51. C. Michard, P. Doublet, Post-translational Modifications are Key Players of the Legionella
654   pneumophila Infection Strategy. *Front. Microbiol.* **6**, 87 (2015).
655 52. X. Guo, Y. Dong, S. Yin, C. Zhao, Y. Huo, L. Fan, H. Hu, Patulin induces pro-survival
656   functions via autophagy inhibition and p62 accumulation. *Cell Death & Disease* **4**, e822-
657   e822 (2013).

53. Y. R. Lee, S. H. Kuo, C. Y. Lin, P. J. Fu, Y. S. Lin, T. M. Yeh, H. S. Liu, Dengue virus-induced ER stress is required for autophagy activation, viral replication, and pathogenesis both in vitro and in vivo. *Sci Rep* **8**, 489 (2018).

54. T. S. Fung, D. X. Liu, The ER stress sensor IRE1 and MAP kinase ERK modulate autophagy induction in cells infected with coronavirus infectious bronchitis virus. *Virology* **533**, 34-44 (2019).

55. X. H. Fun, G. Thibault, Lipid bilayer stress and proteotoxic stress-induced unfolded protein response deploy divergent transcriptional and non-transcriptional programmes. *Biochim Biophys Acta Mol Cell Biol Lipids* **1865**, 158449 (2020).

56. F. Sherman, G. R. Fink, J. B. Hicks, *Methods in Yeast Genetics: Laboratory Course Manual for Methods in Genetics*. (Cold Spring Harbor Laboratory, Cold Spring Harbor, NY, 1986).

Author contributions: RNA-sequencing experiments were performed by N.J.D. Analysis of RNA sequencing data as well as IPA network and pathway analysis was performed by M.K. and N.J.D. Quantitative RT-PCR experiments were carried out by N.J.D. MEF infections and Westerns were carried out by N.J.D, A.E.L, A.K.C., and F.S.C. Yeast strains were prepared by A.K.C. and IRE1-GFP clustering assays were performed by A.K.C and N.J.D. Synteny analysis was carried out by L.N.K. The manuscript was written by N.J.D. and A.K.C. with substantial contributions from K.O. Figures were prepared by N.J.D, M.K., A.K.C and L.N.K. The research was funded by grants to K.O., C.X. and N.V.G.

687

Competing interests: The authors declare no competing financial interests

689

Data and materials availability

The authors declare that the data supporting the findings of this study are available within the paper and the Supplementary Information. Complete RNA-sequencing data has been deposited on the Gene Expression Omnibus server (GSE120273). All data is available from the corresponding author upon request.

695

Figure Legends:

Figure 1. VopQ and VopS have antagonistic effect on T3SS1-specific pathway and network induction.

Figure 2. VopQ but not VopQ^{S200P} induces an early activation of ERK1/2 MAPK signaling.

Figure 3. Activation of ERK1/2 MAPK signaling by VopQ is dependent on IRE1 activation.

Figure 4. Activation of ERK1/2 MAPK signaling by VopQ is dependent on IRE1 kinase activity

704

705

706

707   **Figures:**

708

709   **Figure 1. VopQ and VopS have antagonistic effect on T3SS1-specific pathway and network**

710   **induction. A)** Illustration of temporal effector function during T3SS1-mediated cell death **B)**

711   Heatmap of normalized differential expression of previously identified T3SS1-specific

712   transcripts in uninfected (UN) primary human fibroblasts compared to primary human fibroblasts

713   infected with either *V. para* T3SS1$^+$, T3SS1$^+\Delta vopQ$, or T3SS1$^+\Delta vopS$ for 90 minutes. Yellow

714   denotes transcripts with relative increased abundance infected cells compared to UN cells, and

715   blue denotes a decreased abundance. Clusters (color bars on the left) were assigned through

716   hierarchical clustering of the differential expression data. **C)** Heatmap of predicted repression

717   (blue) and activation (yellow) Z-scores calculated from differential expression data for UN vs. *V.*

718   *para* T3SS1$^+$, UN vs. *V. para* T3SS1$^+\Delta vopQ$, and UN vs. *V. para* T3SS1$^+\Delta vopS$ using

719   QIAGEN's Ingenuity$^®$ Pathway Analysis software. The color key correlates the displayed

720   heatmap color and calculated Z-scores and gray denotes unaffected (*p*>0.05) pathways. **D)**

721   Heatmap of Ingenuity$^®$ Pathway Analysis Z-score prediction of repression (blue) or activation

722   (yellow) of biological networks after 90 minutes of POR3:T3SS1$^+$, T3SS1$^+\Delta vopQ$, and

723   T3SS1$^+\Delta vopS$ infection.

724

725

726

727

728

729 **Figure 2. VopQ but not VopQ^{S200P} induces an early activation of ERK1/2 MAPK signaling.**

730 **A)** Immunoblot showing phosphorylated Erk1 and Erk2 (p-Erk1/2) and total Erk1/2 in starved

731 mouse embryonic fibroblasts (MEFs) 45, 60, 75 and 90 minutes post-infection with T3SS1^{+} or

732 T3SS1^{-} *V. para*. A pulse of p-Erk1/2 was observed early during infection with T3SS1^{+} but not

733 T3SS1^{-} *V. para*. **B)** Immunoblot for total Egr1 in starved MEFs 45, 60, 75 and 90 minutes post-

734 infection with POR3:T3SS1^{+} or POR3:T3SS1^{-}. A rise in Egr1 protein levels over time is

735 observed only in T3SS1^{+}-infected MEFs. **C)** Immunoblot for p-Erk1/2 and total Erk1/2 in

736 starved MEFs 45, 60, 75 and 90 minutes post-infection with T3SS1^{+}Δ*vopQ* or T3SS1^{+}Δ*vopS V.*

737 *para*. T3SS1^{+}Δ*vopQ* does not induce Erk1/2 phosphorylation while T3SS1^{+}Δ*vopS* induces

738 prolonged Erk1/2 phosphorylation. **D)** Immunoblot for total Egr1 in starved MEFs 45, 60, 75 and

739 90 minutes post-infection with *V. para* T3SS1^{+}Δ*vopQ* or T3SS1^{+}Δ*vopS*. No rise in Egr1 protein

740 levels is observed in T3SS1^{+}Δ*vopQ*-infected MEFs while T3SS1^{+}Δ*vopS* causes an increase in

741 Egr1 protein levels. Target band marked with a red line and background bands with a blue star.

742 **E)** Immunoblot showing p-Erk1/2 and total Erk1/2 in starved MEFs infected with T3SS1^{+},

743 T3SS1^{+}*vopQ*^{S200P}, T3SS1^{+}Δ*vopQ,* and T3SS1^{+}Δ*vopQ*+p*vopQ V. para* strains for 45, 60, 75 and

744 90 minutes. No pulse of pERK1/2 is observed in T3SS1^{+}*vopQ*^{S200P}-infected MEFs. **F)**

745 Immunoblot for total Egr1 in starved MEFs infected for 45, 60, 75 and 90 minutes with the same

746 *V. para* strains as in 3E T3SS1^{+}*vopQ*^{S200P} does not trigger an increase Egr1 protein levels in

747 infected MEFs. Target band marked with a red line and background bands with a blue star. Blots

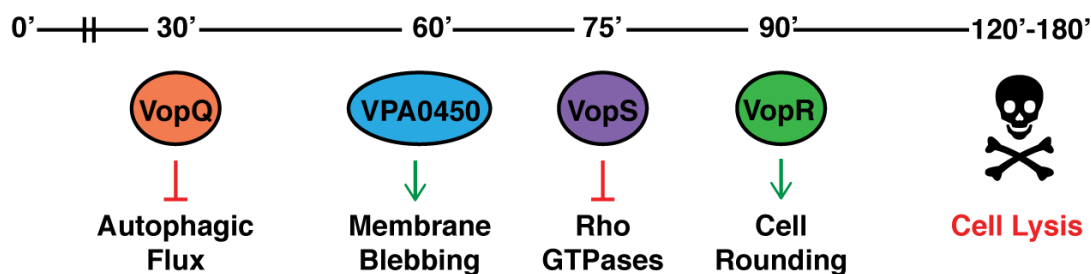748 are representative of N=3 independent experiments.

749

30

Figure 3. Activation of ERK1/2 MAPK signaling by VopQ is dependent on IRE1 activation. A) Immunoblots for total Egr1, p-Erk1/2, and total Erk1/2 in starved wild-type (WT) and *Ire1*$^{-/-}$ MEFS infected for 45 and 60 minutes with *V. para* T3SS1$^+$ or *V. para* T3SS1$^-$. Erk1/2 phosphorylation and increased Egr1 protein levels are not observed in *Ire1*$^{-/-}$ MEFS. **B)** Immunoblots for total Egr1, p-Erk1/2, and total Erk1/2 in starved *Atf6*$^{-/-}$ and *Perk*$^{-/-}$ MEFS infected for 45 and 60 minutes with *V. para* T3SS1$^+$ or *V. para* T3SS1$^-$. **C)** Immunoblots for total Egr1, p-Erk1/2, and total Erk1/2 in starved (-) or FBS-stimulated (+) WT, *Ire1*$^{-/-}$, *Atf6*$^{-/-}$ and *Perk*$^{-/-}$ MEFS. Target band is marked with a red line and background bands with a blue star. Blots are representative of N=3 independent experiments. **D)** Representative micrograph of Ire1p-GFP cluster formation in yeast after 45 minutes of DTT treatment or effector expression. Scale bar is 5 microns **E)** Quantification of **D**. Average percent of cells (n=100) with Ire1p-GFP foci from N=3 independent experiments. Error bars represent ±SEM. *p*-values were calculated by unpaired t test (****$p<0.0001$).**F)** Immunoblot for p-Ire1α and total Ire1α in MEFs infected with T3SS1$^+$, T3SS1$^+\Delta vopQ$, T3SS1$^+\Delta vopQ$+p*vopQ*, and T3SS1$^+vopQ^{S200P}$ *V. para* strains for 45 and 60 minutes. Target band marked with a red line and background bands with a blue star. Blots are representative of N=3 independent experiments.

773

774

775   **Figure 4. Activation of ERK1/2 MAPK signaling by VopQ is dependent on IRE1 kinase**

776   **activity. A)** Immunoblots for total Egr1, p-Erk1/2, and total Erk1/2 in starved wild-type (WT)

777   MEFS untreated or treated with 4μ8c or KIRA6 inhibitors for 24 hours and 1 hour, respectively

778   and infected for 45 and 60 minutes with *V. para* T3SS1$^+$ or *V. para* T3SS1$^-$. Erk1/2

779   phosphorylation and increased Egr1 protein levels are not observed in MEFS treated with

780   KIRA6 kinase inhibitor. Blots are representative of N=3 independent experiments. **B)** Model for

781   IRE1-dependent modulation of Erk1/2 MAPK signaling by VopQ and VopS during *V. para*

782   infection. Green arrows indicate activation and red lines depict inhibition. Dashed lines indicate

783   postulated connections in the model requiring future study. Specifically, it is possible that Rho

784   GTPases may be upstream of Ire1 and how VopQ's inhibition of autophagic flux affects Ire1
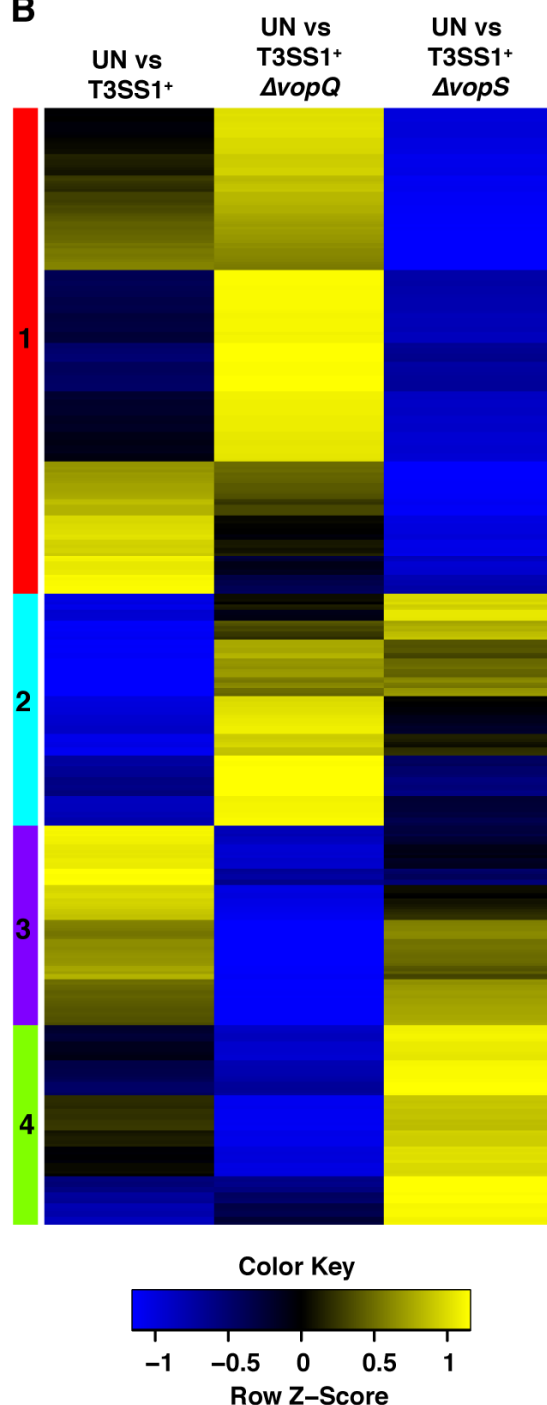
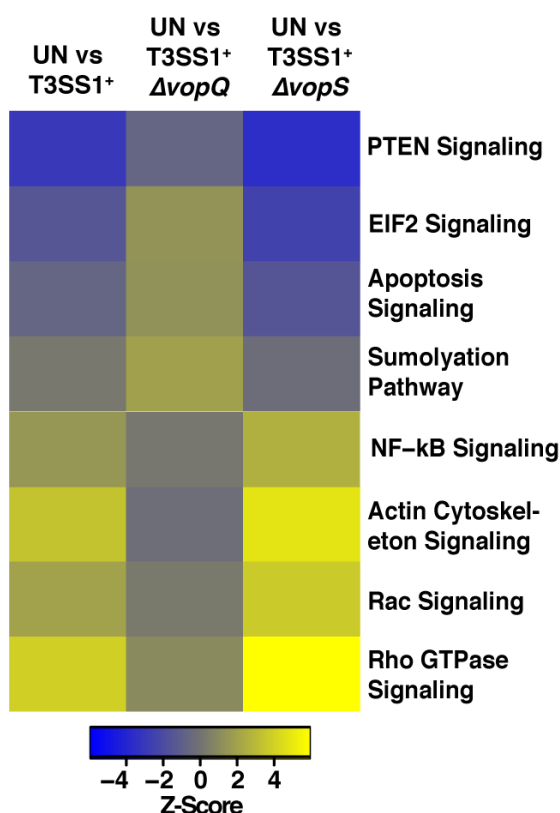785   signaling and vice versa is unclear.
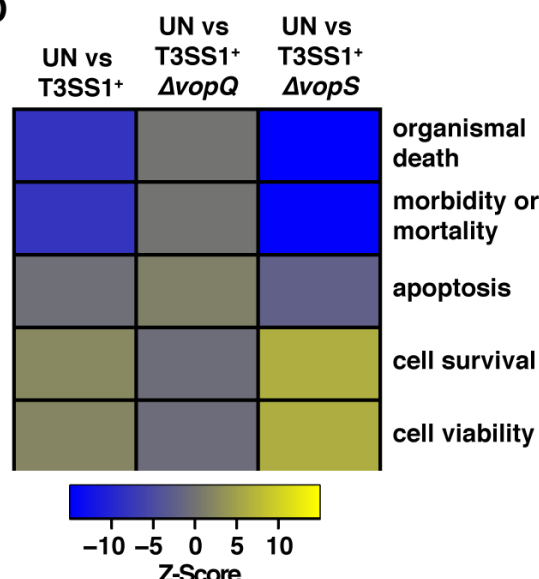
786

A

V. para T3SS1⁺ infection timeline

0' — 30' — 60' — 75' — 90' — 120'-180'

VopQ ⊣ Autophagic Flux

VPA0450 ↓ Membrane Blebbing

VopS ⊣ Rho GTPases

VopR ↓ Cell Rounding

Cell Lysis

B

UN vs T3SS1⁺ | UN vs T3SS1⁺ ΔvopQ | UN vs T3SS1⁺ ΔvopS

1
2
3
4

Color Key

−1 −0.5 0 0.5 1
Row Z−Score

C

UN vs T3SS1⁺ | UN vs T3SS1⁺ ΔvopQ | UN vs T3SS1⁺ ΔvopS

PTEN Signaling
EIF2 Signaling
Apoptosis Signaling
Sumolyation Pathway
NF−kB Signaling
Actin Cytoskeleton Signaling
Rac Signaling
Rho GTPase Signaling

−4 −2 0 2 4
Z-Score

D

UN vs T3SS1⁺ | UN vs T3SS1⁺ ΔvopQ | UN vs T3SS1⁺ ΔvopS

organismal death
morbidity or mortality
apoptosis
cell survival
cell viability

−10 −5 0 5 10
Z-Score

Color Key

Color Key